Numerical Analysis of Steady Current and Temperature Distributions and Characteristics of Transverse Mode in VCSEL [*]

Liu Shian (   ), Lin Shiming (   ), Kang Xuejun (   ),
Cheng Peng (   ), Lu Jianzu (   ), Wang Qiming (   )

(National Key Laboratory of Integration Opto-electronic Technology, Institute of
Semiconductors, The Chinese Academy of Sciences, Beijing   100083)

Abstract   The eigen transverse modes of the cylindrical Vertical-Cavity Surface-Emitting Laser (VCSEL) are investigated by numerical simulation. The steady current and temperature distributions in the cavity are calculated self-consistently by the finite element method. At the steady state, the solution of the transverse mode equation in the active region is obtained by the matrix eigenvalue method, taking the material thermal properties and all the significant heat resources into consideration. The output light patterns above the threshold current are also demonstrated in this paper.

1 Introduction

In the past few years, the Vertical-Cavity Eurface-Emitting Lasers (VCSEL) was improved considerably in its performance due to the introduction of the intracavity dielectric aperture for the electrical and optical confinement, which was normally formed by the non-conductive Al_xO_y from the selective wet oxidation of AlAs [1,2] Because the gain-wave guide structure of the VCSEL is rather weak, J. P. Zhang[3], Y. S. Zhang[4] and Morozov et al [5] drew a conclusion that the transverse mode was affected by the gain-distribution in the active layer. Rahman et al [6] noticed the effects of the carriers distribution on the transverse mode. And the thermal effects in the cavity were discussed by Zhang. [7] They took these effects into account separately, but in fact these factors took effects simultaneously. The current (or the driving carriers) distribution is the basic characteristic of an optoelectronic device, but the thermal property plays a significant role as well because of the non-omission of its effect on the gain-distribution in the small cavity. The VCSEL trans-

verse-m ode can be obtained from the solution of M axw ell equations in the gain-w ave guide cavity.   In this paper, the V CSEL simulation is presented and the current distribution, the them al distribution and the optical transverse mode are concerned in the steady state.   The finite element method, the finite difference method and the matrix eigenvalue method are used to obtain above distributions and the eigen mode.   A s a result, the distributions of the current, temperature and light power in the cavity are presented at the different driving currents under the confinem ent conditions

2   Calculation M odel

The schem atic diagram of the cylindrical V CSEL cavity is show ed in Fig. 1. W_0 is the diam eter of light outputw indow , R_0 is the radius of a cavity, a_0 is the radius of a current w indow .   The transverse modes are determ ined by the follow ing factors
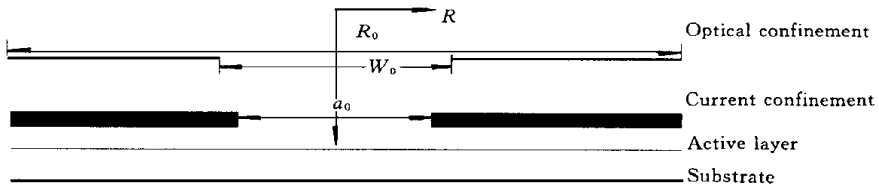

F IG. 1   Schem atic diagram of a V CSEL

2. 1   The current d istribution

A t the steady state, once the bias-voltage is given, the static distribution of the current is determ ined by M axw ell equations and the boundary conditions   It can be form ulated by using the conventional (r, θ, z) on cylindrical coordinates   Due to the axis symm etric structure of the V CSEL , the 3-dimension equation is reduced to a two-dimension one, w ith the current being the solution of the equation

$$\begin{cases} \dfrac{\partial^2 V}{\partial r^2} + \dfrac{1}{r} \dfrac{\partial V}{\partial r} + \dfrac{\partial^2 V}{\partial z^2} = 0, \\ \vec{j} = - \sigma(\vec{r}) \, \nabla V(\vec{r}), \end{cases} \tag{1}$$

w here $\sigma(r)$ is the conductivity distribution in the cavity.

2. 2   The thermal d istribution

In the cylindrical coordinates, the basic heat equation given w hich governs the steady-state heat flow by Poisson equation.

$$\nabla[\kappa(r) \cdot \nabla T(r)] = - Q(r), \tag{2}$$

W here $T(r)$, $Q(r)$ *and* $\kappa(r)$ are respectively the spatial variations of the temperature, the internal heat sources and the material them al conductivity.   The follow ing assumptions are applied: (1) at the bottom junction betw een the V CSEL substrate and the heat sink, w hich contacts w ith the V CSEL substrate, the temperature is keeping constant, $T = T_0$;

(2) at the top or the side wall with adiabatic conduction, $\frac{\partial T}{\partial r}\Big| = 0$. Besides, there are two types of heat soucrces:

(i) the heat generated in the active region by nonradiation recombination

$$q(r) = \frac{U(r)(1 - \eta_{sp}f_{sp})}{d}[j_{th} + (j(\vec{r}) - j_{th})(1 - \eta)]. \tag{3}$$

(ii) the Joules heat in the other regions

$$q(\vec{r}) = j(\vec{r})^2 \cdot \rho(\vec{r}), \tag{4}$$

Where $U(r)$ and $j(r)$ are the voltage drop and the current density in the quantum well (QW) region. While $j_{th}(r)$, η_{sp} and f_{sp} are the threshold current density, the internal quantum efficiencies of spontaneous and the stimulated emission, respectively. When the driving current is at equal to or higher than the threshold, the voltage drop $U(r)$ can be regarded as a constant $U = V_g$. V_g is the build-in field. For GaAs, $V_g = 1.2$ eV.

2.3 The carriers distribution in the active region

The carriers enhance the gain in the active region then form a gain wave guide to modify the transverse mode of the laser. Because the QW's width, 8nm, is much less than the effective length of the cavity, the distribution equation can be reduced into one-dimension

$$D_n \nabla^2 N(\vec{r}) - \frac{N(\vec{r})}{\tau_s} - v_g\Gamma_r g(N(\vec{r}))\sum_i P_i = -\frac{J(\vec{r})}{ed}, \tag{5}$$

D_n, v_g, Γ_r and τ_s are the diffusion coefficient of the carriers, the group velocity of the light wave in the cavity, the confinement factor and the lifetime of the carrier, respectively. P_i is the photon energy for the i-th mode; $g(N)$ is the gain of the cavity, depending on the carriers density.

$$g(N(\vec{r})) = a(T) \cdot (N(\vec{r}) - N_{th}), \tag{6}$$

N_{th} is the density of the transparent carriers.

2.4 Optical field

The optical property is mainly determined by the gain profile, the carrier distribution and the temperature distribution in the active region. As assumed above, it can also be reduced into one-dimension. The p-th mode of light is the solution of the wave equation

$$\frac{1}{r}\frac{\partial}{\partial r}\left(r\frac{\partial\Psi}{\partial r}\right) + \left[k_0^2\frac{\epsilon}{\varepsilon} - \frac{m^2}{r^2} - \beta_z^2\right]\Psi = 0 \tag{7}$$

$$\Phi(\theta) = \frac{1}{\sqrt{2m}}e^{im\theta} \tag{8}$$

Where k_0 is the plane wave vector, β_z is the complex propagation constant in the z direction. Where ϵ and ε are the complex dielectric constant and the vacuum dielectric constant respectively.

$$\frac{\epsilon}{\varepsilon} = n_0^2 + 2(\delta n)n_0 + i\frac{[g(\vec{r}) - a_{total}]}{2k}, \tag{9}$$

where n_0, g and α_{total} are dielectric refraction index, gains and total losses of the cavity respectively.

The param eters refer-
enced in this paper are list-
ed in Table 1. N , q_e and ω
are the carriers' density,
electronic charge, and the
frequency of the light n_0,
and m_0 are the effective in-
dex of the active layer and
the effective m ass of the
carrier.

Table 1

Parameter		Value
V_g	the group velocity	8×10^9 cm/s
q_e	electronic charge	1.6×10^{-9} C
N_{th}	transparent carriers density	1.5×10^{18} cm^{-3}
D_n	carrier diffusion coefficient	4.8×10^{-2} cm/s
τ_c	carriers life time	2 ns
R_1, R_2	reflect coefficient for top and bottom DBR	0.99, 1.0
d	width of the well	8nm
σ_1	conductivity of the confinement region	$10^{-1} \Omega^{-1} \cdot$ cm^{-1}
σ	conductivity of other regions	$5 \times 10^2 \Omega^{-1} \cdot$ cm^{-1}
ω	frequency of the light	3×10^{14} Hz

3   Calculation m ethod

T hree   calculation
m ethods w ere adop ted in this sim ulation: the finite elem ent m ethod （FEM ）, the finite dif-
ference m ethod （FDM ） and the m atrix eigen m ethod The finite elem ent m ethod[8] is a
pow erful engineering tool for its flexibility and versatility, especially in com plicated
boundary structure It w as em ployed to solve the electric and heat distribution equations
In this procedure, the concerned structure w as first autom atically divided into sm all subre-
gions, triangle elem ents W ith these elem ents, the com plicated structure of the cavity can
be m odulated The m em ory requirem ent of the FEM program does not beyond 32M b to a
general personal com puter for the safe w ork of the system.   In the finite elem ent m ethod,
the 2-dim ension Poisson s equation could be expressed as follow ing m atrix equation.

$$[K] \cdot [\Psi] - [P] = [0], \tag{10}$$

$[K]$ is a structure factor, w hich could be obtained from com bination w ith the finite ele-
m ents $[\Psi]$ is the distribution of the field and $[P]$ is the field resource The elem ents of
m atrix $[K]$ are obtained through the follow ing expressions

$$K_{ii} = \sum_i k_{ii}^e \qquad K_{ij} = \sum_{ij} k_{ij}^e, \tag{11}$$

i is the summ ation of the triangle elem ents having the common vertex;   ii is the sum -
m ation of the triangle elem ents having the common hypotenuse.

The them al distribution w as obtained by the traditional FEM. W ithout the source in
the electric field, the electric equation w as reduced to L aplace equation The carrier distri-
bution equation w as treated upon FDM [9] and the Optical field equation w as reduced to a
set of linear equations, w hich w as treated by the m atrix eigen process[10]. The final results
w ere obtained by recursion self-consistently. The output of the n step w as set as the input
of the $n+1$ step. A nd the stepped calculation w ould be stopped until the difference of re-
sults betw een two continuous steps is less than 0.01%.

4   Num erical Results

Two structures, w ith the current confinem ent w indow radii, 2μm and 10μm respec-

tively, are simulated as the examples The used structure parameters are given in Table 2

Table 2

Parameter		Value
R_0	radii of the cavity	15μm
L_{eff}	effective length of the cavity	1.5μm
w_0	the radii of the light-output window	6μm
d	the position of resistance region	0.6μm

The results show that the threshold of first structure was reduced to 0.515 mA, while that of the second was 1.47mA. However, the current densities in the active regions reach 2500 A/cm^2 and 1300 A/cm^2 for the strong and weak confinement structures respectively. The contour map of the confined cavity is presented in Fig. 2 and Fig. 3
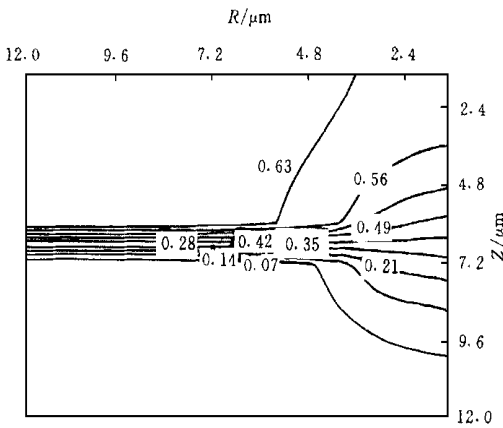
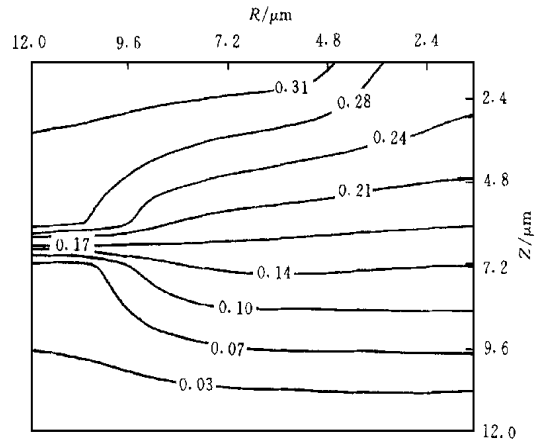FIG. 2   The contour map of the electric field of
the strong confinement structure

FIG. 3   The contour map of the electric field of
the weak confinement structure

Fig. 4 and Fig. 5 (see last page Ⅰ) respectively show the output pattern of light intensity for two structures, when the current I is 3 times of the threshold current I_{th} The output pattern as the transverse mode is the numerical result of the optical equation in the active layer. In our model, all the gain-guide elements were treated numerically, and the eigen transverse mode series contain the modes which are like the ground and the first mode, not same as the existing of higher mode that in the dielectric guide But for the weak confinement one, the output pattern is concentrated in the center.

Fig. 6 and Fig. 7 (see last page Ⅰ) show the current density distributions in the cavity. The strong confinement benifits to concentrate the current density in the active region to a higher level, at the same time of the reduction of the threshold.

The temperature distributions are also presented in Fig. 8 and Fig. 9 (see last page Ⅱ). In Fig. 7, the current peak is far away from the heat peak, which means that the heat resource is dominated by the non-radiation process The temperature peak of the strong confined structure is slightly higher than the weak one, though the average temperature is lower than the latter.

With the increment of the driving current, the hole-burning takes place. At about 5I_{th} it appears in the output pattern of the weak confinement device while at about 6I_{th} in the

strong one. The confinem ent ham pers the ho le bu rn ing. Fig. 10 and Fig. 11 (see last page II) p rove the output pattern in the bu rn ing-ho le region.

Fu rthem o re, the relation sh ip betw een the th resho ld cu rrent I_{th} and the radiu s W_0 of the confine m ent w indow is fitted.

In F ig. 12, I_{th} can be given as the function of W_0

$$I_{th} = -\frac{0.00288}{1 + \left(\dfrac{W_0}{x_0}\right)^p} + 0.00333, \quad (12)$$

FIG. 12   The th resho ld current I_{th} as the function of the radii of the confinem ent w indow W_0

w here $x_0 = 12.87454$, $p = 2.33218$. Th is resu lt ag rees very w ell w ith the experim en tal resu lts of O h. [11]

5   Conclusion

O u r sim u lating resu lts dem on strate several characters of V CSEL at steary state. The key ro le of the h igh resistance confinem en t layer is p resen ted clearly. The strong confined structu re no t on ly focu ses the cu rrent, but also com pacts the cu rrent pattern effectively. B ecau se it concentrates the cu rrent den sity in the active region (Fig. 7) to a h igher level, the th resho ld cu rrent is reduced and the ho le bu rn ing is ham pered do fu rther. The o ther dynam ic effects such as m icrocavity effect *et al.* , w ill be con sidered in fu tu re sim u lation.

References

[1]   R. S. Geels *et al.* , A pp l Phys L ett. , 1990, **57**: 1605.
[2]   Chang-Hasnain *et al.* , A pp l Phys L ett. , 1990, **57**: 1307.
[3]   J. P. Zhang, IEE P roc J, Op toelectron. , 1995, **142**(2): 87.
[4]   Y. S. Zhang *et al.* , Ch inese Jou rnal of Sem iconducto rs, 1998, **19**(1): 29.
[5]   V. N. M o rozov *et al.* , IEEE J. Q uantum E lectron. , 1997, **33**(6): 980.
[6]   B. M. A. Rahm an *et al.* , IEE P roc. J, Op toelectron. , 1995, **142**(2): 82.
[7]   J. P. Zhang *et al.* , IEE P roc J, Op toelectron. , 1995, **142**(1): 29.
[8]   , ,   , :   , 1984
[9]   , C   , :   , 1994
[10]   , , FORTRAN   , :   , 1982
[11]   T. H. O h *et al.* , A pp l Phys L ett. , 1996, **69**(21): 3152

L iu Shi'an（　　　）*et al.* : 　Numerical Analysis of Steady Current and Temperature Distributions and Characteristics of Transverse Mode in VCSEL
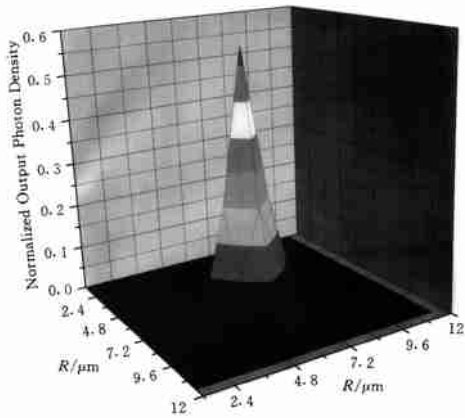
Last Page Ⅰ

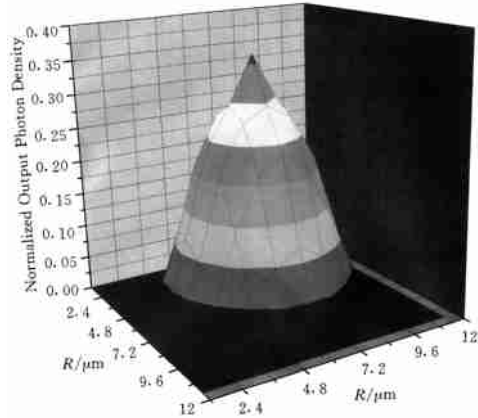FIG 4　The output photon density distribution of the strong confinement structure at $I=3I_{th}$

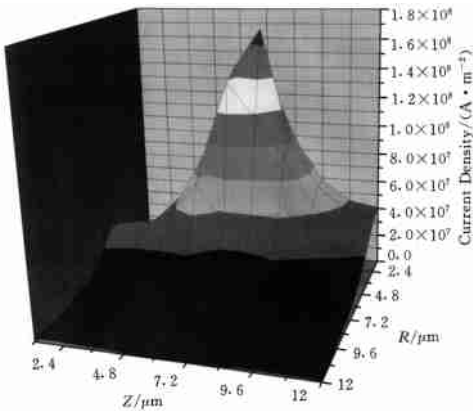FIG 5　The output photon density distribution of the weak confinement structure at $I=3I_{th}$

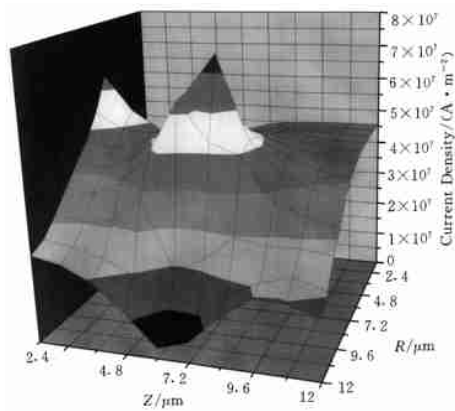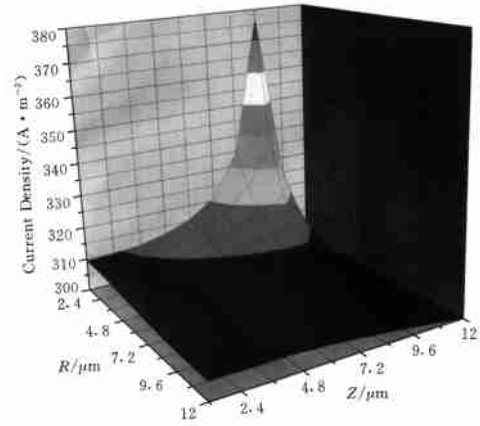FIG 6　The current density distribution of the strong confinement structure at $I=3I_{th}$

FIG 7　The current density distribution of the weak confinement structure at $I=3I_{th}$

FIG. 8　The temperature distribution
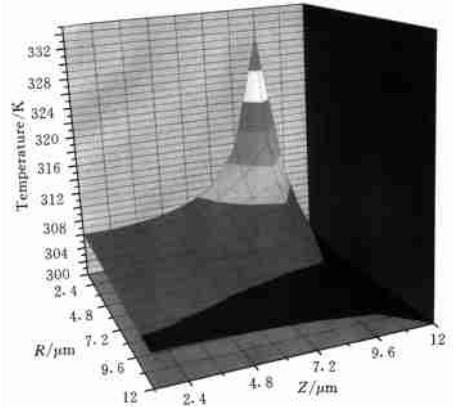of the strong confinement
structure of $I = 3I_{th}$

FIG. 9　The temperature distribution
of the weak confinement
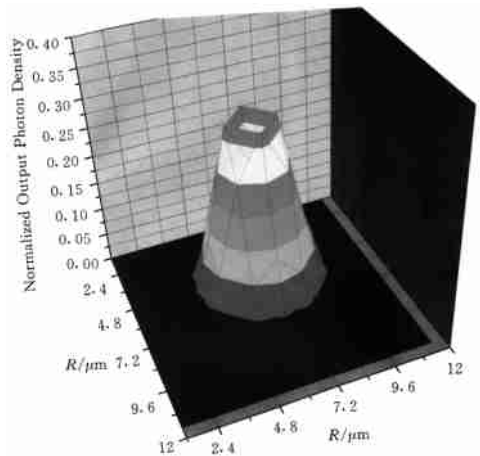structure of $I = 3I_{th}$

FIG. 10　The output photon density
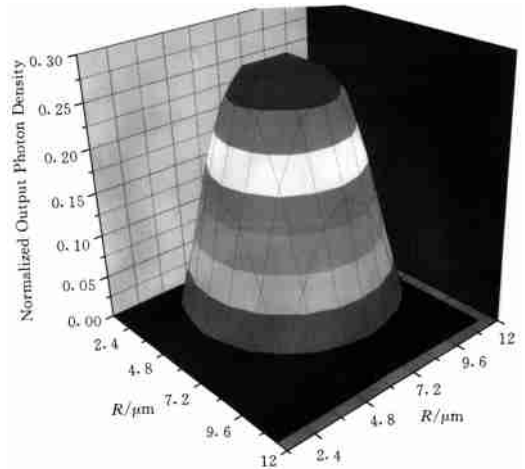distribution of the strong confinement
in the burning-hole region.

FIG. 11　The output photon density
distribution of the weak confinement
structure in the burning-hole region.